American Mineralogist, Volume 88, pages 450–461, 2003

Another step toward understanding the true nature of sartorite: Determination and refinement of a ninefold superstructure

PETER BERLEPSCH,[1,*] THOMAS ARMBRUSTER,[1] EMIL MAKOVICKY,[2] AND DAN TOPA[3]

[1]Laboratorium für chemische und mineralogische Kristallographie, Universität Bern, Freiestrasse 3, CH-3012 Bern, Switzerland
[2]Geological Institute, Department of Mineralogy, University of Copenhagen, Øster Voldgade 10, DK-1350 Copenhagen K, Denmark
[3]Departement für Geologie und Mineralogie, Universität Salzburg, Hellbrunner Str. 34/III, A-5020 Salzburg, Austria

ABSTRACT

Single-crystal X-ray diffraction data, collected from a sartorite crystal from Lengenbach (Binntal, Valais, Switzerland), yielded a ninefold superstructure: space group $P2_1/c$; $a = 37.71(2)$, $b = 7.898(3)$, $c = 20.106(8)$ Å, $\beta = 101.993(7)°$; $R_1 = 6.08\%$ for 6293 reflections with $I > 2\sigma_I$. The sample is an $N_{1,2} = 3,3$ sartorite homologue and the refined formula $Pb_8Tl_{1.5}As_{17.5}S_{35}$ compares very well with the empirical formula $Pb_{8.2}Tl_{1.4}As_{17.5}Sb_{0.5}S_{35}$ obtained from electron microprobe analyses. It has a high Tl content, up to 6.5 wt%. In a coupled substitution approximately 1.5 Tl^+ replace about 0.5 As^{3+} and 1 PbS. The refined structure has 35 S atoms pfu instead of the expected 36 S (= 9 × 4 S, from $PbAs_2S_4$). The incorporation of substantial amounts of Tl^+ into $PbAs_2S_4$ is essential for the type and periodicity of superstructures in sartorite. The refined superstructure can be interpreted as a so-called "lock-in" structure with a composition that yields a commensurate lattice for a mineral that usually has an incommensurate lattice. No commensurate periodicity could be found for a second crystal with about 0.5 Tl apfu.

INTRODUCTION

Sartorite, with simplified formula $PbAs_2S_4$, has long been known to occur only at the Lengenbach deposit, Binntal (Valais, Switzerland), where it is the most common Pb-As-S sulfosalt. Anthony et al. (1990) gave two additional localities for sartorite: the Zuni mine (Colorado) and the Pitone marble quarry (Apuane Alps, Italy). The mineral sartorite was first described under the name scleroclase by Walterhausen (1857; in Palache et al. 1944); subsequently G. vom Rath (1864) proposed the name sartorite, for Sartorius Walterhausen, and this has gained general acceptance (Palache et al. 1944). The simple stoichiometry of sartorite, $PbAs_2S_4$, belies the complexity of its true nature. Early crystallographers (Baumhauer 1895; Solly and Jackson 1902; Trechmann 1907) failed to find a consistent set of axial ratios that would satisfactorily index all observed morphological forms. The X-ray diffraction studies of Bannister et al. (1939) showed sartorite to be monoclinic but with a strong orthorhombic subcell (Table 1). Nowacki et al. (1961) confirmed the orthorhombic subcell but they found a different monoclinic supercell (Table 1). Nowacki et al. (1961) solved and refined the sartorite structure on a subcell level with the monoclinic space group $P2_1/n$ with $\beta = 90°$, but they did not attempt to solve their $3a \times b \times 11c$ superstructure. Iitaka and Nowacki (1961) further refined the substructure, but not to their complete satisfaction. They curtailed their refinement at $R = 14.7\%$, leaving several aspects of the structure unclear.

Although only the substructure of sartorite was solved (Nowacki et al. 1961; Iitaka and Nowacki 1961), the basic building principles of this mineral were clear. In addition, Le Bihan (1962) reported on crystal structures of compounds structurally and chemically related to sartorite. These compounds, as well as those (re-)investigated primarily by Nowacki's group in the 1960s, became the basis of what Makovicky (1967, 1985) later contributed to, and described as, the sartorite homologous series.

The sartorite homologues are a series of Pb-As sulfosalts with zigzag walls composed of columns of "standing" tricapped trigonal coordination prisms of Pb (coordination number 9 = CN9) that alternate with variously thick slabs composed of "lying" monocapped trigonal coordination prisms of As and Pb (CN7); these slabs are based on the SnS-archetype. The structure of the sartorite homologues can be visualized as being composed of slices of SnS-like structure cut parallel to the $(301)_{SnS}$ or $(30\bar{1})_{SnS}$ planes (e.g., Fig. 9 in Makovicky 1997). These slices include polyhedra from both the walls and the slab and are $N = 3$ to 4 polyhedra thick (Makovicky 1985).

The crystal chemistry of the sartorite homologues was worked out by Nowacki's school (e.g., Nowacki et al. 1960, 1961; Iitaka and Nowacki 1961), by the comparative analysis of Makovicky (1985), and by the coordination analysis of Berlepsch et al. (2001). Pring (2001) unravelled the complex HRTEM architecture of the sartorite group. Electron diffraction studies performed by Pring et al. (1993) on sartorite showed satellite reflections that were generally incommensurate with respect to the subcell $a = 19.62$, $b = 7.89$, $c = 4.19$ Å, $\beta = 90°$ and space group $P2_1/n$. However, in some crystal fragments the primary modulation wave vector is "locked in" along [101], giving a commensurate superstructure, the unit cell of which is obtained by the transformation matrix $R = [10–1, 010, 0.0.13]$

* E-mail: peter.berlepsch@krist.unibe.ch

TABLE 1. Selected unit cell data of sartorite (sub- and supercells) reported in the literature (dimensions given in Å)

Subcell				Supercell					
a 19.46	*b* 7.79	*c* 4.17		$P2_12_12_1$	3*a*	*b*	20*c*			(1)
a 19.48	*c* 7.86	*b* 4.15		$P2_12_12_1$	3*a*	*b*	20*c*		$P2_12_12_1$	(2)
a 19.62	*b* 7.89	*c* 4.19		$P2_1/n$	3*a*	*b*	11*c*	β = 90°	$P2_1/n$	(3)
a 19.6	*b* 7.9	*c* 4.2		*Pbnm*	3*a*	*b*	11*c*			(4)
a' 20.06	*b* 7.89	*c* 4.19	β = 102.1°	$P2_1/c$	3a'–8c	*b*	11*c*	β = 128.1°		(4)
a 19.62	*b* 7.89	*c* 4.19	β = 90°	$P2_1/n$						(5)
a' 20.11	*b* 7.90	*c* 4.19	β = 102.0°	P2$_1$/c	9*c*	*b*	*a*'	β = 102.0°	$P2_1/c$	(6)

Notes: The matrix for transforming the $P2_1/n$ unit-cell setting into $P2_1/c$ is: R = [101, 0-10, 00-1]; *a*' indicates the $P2_1/c$ setting. References: (1) Bannister et al. (1939); (2) Berry (1943); (3) Iitaka and Nowacki (1961), Nowacki et al. (1961); (4) Ozawa and Takéuchi (1993); (5) Pring et al. (1993); (6) this study.

(Table 1). Pring et al. (1993) suggested that the structural modulation is associated with displacements of atoms in the As-S chains around the $(101)_{subcell}$ planes. The As-S chains running parallel to $[001]_{subcell}$ are divided into segments by displacement of the S atoms toward the $(101)_{subcell}$ planes.

The number of sartorite homologues has steadily expanded in the past and new phases have been added. Theoretically there are four ways in which the theme can be varied: (1) alteration of the slab thickness to a value other than N = 3 or 4 (not yet observed); (2) chemical substitution, e.g., in the Tl-Sb-S and Ba-Sb-S compounds related to the sartorite homologues; (3) a combinatorial series (Makovicky 1985) of the two hitherto observed module combinations, as in liveingite (N_{1-6} = 4,3,4,4,3,4), baumhauerite-2*a* (N_{1-4} = 4,3,4,3), baumhauerite-ψ*O*3*abc* (N_{1-6} = 4,3,4,3,4,3) or in the 115 Å (N_{1-10} = 4,3,4,3,4,4,3,4,4,3,4), and 138 Å (N_{1-12} = 4,3,4,3,4,4,3,4,3,4,3,4) phases; (4) superstructure formation as reported for sartorite in this study. Although the Pb-As-S based sartorite homologues with homologue numbers other than N = 3 or 4 are not known, synthetic $N_{1,2}$ = 3,3 and 4,4 compounds related to the series have been described (e.g., Cordier and Schäfer 1979; Cordier et al. 1984; Berlepsch et al. 1999; Choi and Kanatzidis 2000). Variations in module combinations (i.e., combinatorial series) have been successfully studied by means of HRTEM (e.g., Ozawa and Takéuchi 1993; Pring and Graeser 1994; Ozawa and Tachikawa 1996). Makovicky (1985) pointed out the apparently important role of minor elements Tl and Ag in these compounds; a discussion is given below.

During routine investigations of Lengenbach minerals found in 1993 we discovered sartorite for which a ninefold superstructure (with respect to the subcell structure refined by Iitaka and Nowacki in 1961) could be solved and refined. In this paper we describe the sartorite superstructure and its deviation from the (averaged) substructure. Furthermore, hypothetical models for different possible superstructures are discussed. Special attention is paid to the so-called crankshaft chains (chains of short As-S bonds) and the role of element substitution, which seems to be an essential part of the superstructure formation.

Although the mineral described here most probably fulfills the criteria of a new mineral species, a corresponding proposal has not been submitted to the Commission on New Minerals and Mineral Names (CNMMN) of the International Mineralogical Association (IMA) for the following reasons. First, sartorite crystals are, in general, incommensurate minerals and it was a coincidence that we were able to solve one "lock-in phase." We think that various members of an incommensurate structure series should receive the same name with a crystallographic modifier appended rather than being considered as independent minerals. For "sartorite *sensu stricto*," only the "average structure" (= substructure) is known, the validity of the simple ideal formula is in doubt, and the problems encountered by the morphological crystallographers suggest that all sartorites represent complex structures akin to the one we studied. One can also interpret sartorite minerals as polytypoids with different stacking sequences depending on "minor" chemical substitutions. Chemical differences between different superstructures may be commensurate with errors in microprobe analyses, making the identification by chemical means impossible. From the crystallographic point of view, we were not able to locate a definite Tl site in the structure; Tl seems to be rather disordered.

SAMPLE DESCRIPTION

The crystal fragments used for chemical and structural investigations are dark gray and display red internal reflections. They originate from two samples (LB93502 and LB93512) with crystal aggregates that measure several mm in size and which grew hydrothermally in druses within a white dolomite rock. Macroscopically, sartorite in these samples is associated with realgar (partly transformed into orpiment), dark gray sulfide masses, and pyrite. The latter occurs isolated or as inclusions in sartorite (Fig. 1). Two visually different types of grains were used for both kinds of investigations: (1) two crystal fragments from sample LB93502, which are darker and more opaque than (2) the three less dark and more transparent crystal fragments from sample LB93512. Chemical analyses were performed on all five crystal fragments but only material from sample LB93502 yielded a periodic cell within the resolution of the single crystal X-ray diffractometer setup. No periodic unit cell could be found for a crystal from sample LB93512.

EXPERIMENTAL PROCEDURES

Chemical analyses

Quantitative chemical analyses were performed with a JEOL JXA-8600 electron microprobe (EMP), controlled by a LINK-*eXL* system, operated at 25 kV, 35 nA, and 20 s counting time for peaks and 7 s for background, and a beam diameter of 5 µm. The following standards and X-ray lines were used: galena (PbS: Pb$M\alpha$), lorandite ($TlAsS_2$: Tl$L\alpha$, As$L\alpha$, S$K\alpha$), Ag metal (Ag$L\alpha$), stibnite (Sb_2S_3: Sb$L\alpha$), and chalcopyrite

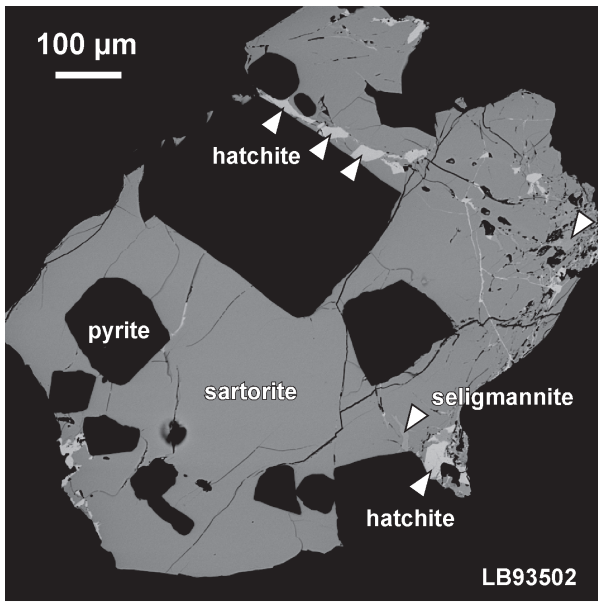

FIGURE 1. Backscattered electron (BSE) image of Tl-bearing sartorite (sample LB93502) with pyrite inclusions (black). Associated minerals are seligmannite ($PbCuAsS_3$, intermediate gray) and hatchite ($PbTlAgAs_2S_5$, light gray).

($CuFeS_2$: Fe$K\alpha$, Cu$K\alpha$). Raw data were corrected with an online ZAF-4 procedure. The results of the sartorite analyses listed in Table 2 are arbitrarily normalized on 35 S atoms pfu because the structure refinement yielded a total of 35 S apfu. Although this procedure makes sense for the composition of the ninefold superstructure, it might be questionable for the other sets of sartorite data because the amount of S depends on the degree of element substitution.

Backscattered electron (BSE) images of the analyzed samples show that the grains from sample LB93512 are homogeneous, although one grain is associated with an Ag-bearing phase, the chemistry of which corresponds to rathite (Table 2). The composition of the rathite is almost identical to those of Laroussi et al. (1989; analysis 38/1), Graeser (in Pring 2001), and Berlepsch et al. (2002). The two grains from sample LB93502 consist of multiple phases (Fig. 1). The matrix of these grains consists of Tl-bearing sartorite (with up to about 6.5 wt% Tl) with inclusions of pyrite. Small inclusions of a slightly brighter phase (in comparison to the matrix) were identified as seligmannite (Fig. 1, Table 2) and the bright inclusions in and on the borders of sartorite were identified as hatchite (Fig. 1, Table 2); both phases appear to replace sartorite. To our knowledge only Laroussi et al. (1989) has published new EMP data for sartorite. All other studies performed on this mineral since the work of Nowacki et al. (1961) lack any data in this respect. Only Graeser (in Hofmann et al. 1993) reports Tl contents in sartorite that exceed 4 wt%, but no details are given. For the sake of completeness, the details from these analyses, performed by A. Edenharter and obtained by courtesy of S. Graeser, have been included in Table 2.

Single crystal X-ray diffraction

An irregular crystal fragment of sartorite of Type 1 (sample LB93502), about $0.18 \times 0.16 \times 0.12$ mm^3 in size, was measured with a Bruker AXS three-circle diffractometer (equipped with a CCD 1000K area detector and a flat graphite monochromator) using Mo$K\alpha$ X-radiation from a fine focus sealed tube (Table 3). The SMART system of programs (Bruker AXS 1998) was used for cell dimension determination and X-ray data collection and the SAINT+ programs (Bruker AXS 1999) were used for data reduction including intensity integration, and background and Lorentz-polarization corrections. The XPREP program (Bruker AXS 1997) was used for empirical absorption correction based on pseudo ψ-scans. The centrosymmetric space group $P2_1/c$ proposed by the XPREP program was chosen, as it is consistent with the monoclinic symmetry of the lattice and intensity statistics $|E^2 - 1| = 1.097$.

Structure determination and refinement

The structure was solved by direct methods with the SHELXS program (Sheldrick 1997a), which revealed about $^3/_4$ of the atom positions. In subsequent refinement cycles, for which we used the SHELXL program (Sheldrick 1997b), additional atomic positions were deduced from the difference Fourier syntheses by selecting from among the strongest maxima at appropriate distances. Subsequently three split cation positions were located. Element attribution at all sites was guided by an analysis of interatomic distances, refinement of individual site occupancies, and the knowledge of the chemical composition based upon the EMP data. However, Tl did not enter the structure refinement since it cannot be distinguished from Pb with the experimental conditions used. The final refinement was performed with anisotropic displacement parameters for all positions (except for M5a and M5b). The occupancies of the split sites were refined, allowing for Pb/As (M5), As/As (As9a, b), and Pb/As (M13) summing to full occupancy. The highest residual peak was 3.04 e/Å^3, 0.84 Å from Pb7 and the deepest hole was –1.80 e/Å^3, 0.89 Å from Pb7 at the end of the refinement. The refinement was stopped when the mean shift/e.s.d. for varied parameters dropped below 1%. Refinement details are listed in Table 3, fractional atomic coordinates and isotropic displacement parameters are given in Table 4, and selected M-S bond distances are condensed in Table 5. Estimated bond valences and selected geometrical parameters, related to individual coordination polyhedra, are summarized in Table 6. Anisotropic displacement parameters and a full list of bond distances and angles have been deposited in Tables 7 and 8[1], respectively.

[1]For a copy of Tables 7 and 8, document item AM-03-023, contact the Business Office of the Mineralogical Society of America (see inside front cover of recent issue) for price information. Deposit items may also be available on the American Mineralogist web site at http://www.minsocam.org.

TABLE 2. Chemical composition of sartorite and associated minerals from Lengenbach

Sample	Phase	N.A.	Pb wt%	Tl wt%	As wt%	Sb wt%	Ag wt%	Cu wt%	Fe wt%	S wt%	Sum wt%
LB93502	seligmannite	1	45.67	0.78	15.84	1.75		14.43	0.03	21.67	100.17
	hatchite	3	24.18	24.40	17.59	1.20	11.20	0.86		19.13	98.54
	sartorite 1a	7	38.06	6.39	29.28	1.42				25.13	100.27
	sartorite 1b	9	38.94	5.77	29.04	1.41				25.01	100.37
LB93512	rathite	6	45.07	0.91	25.52	0.64	3.82		0.04	24.40	100.39
	sartorite 2a	9	44.01	2.13	28.22	0.74				25.21	100.32
	sartorite 2b	7	43.29	2.78	28.49	0.74				25.17	100.46
	sartorite 2c	6	42.83	3.23	28.63	0.79				24.94	100.42
A.E.	Sartorite	20	41.94	4.08	28.48					24.97	99.47
Formulae normalized on: 6 atoms (seligmannite), 10 atoms (hatchite), 35/40 sulfur atoms (sartorite/rathite) per formula unit											
LB93502	seligmannite	1	0.98	0.01	0.94	0.06		1.01	0	3.00	
	hatchite	3	0.98(1)	1.00(0)	1.97(1)	0.08(1)	0.87(0)	0.11(1)		4.99(2)	
	sartorite 1a	7	8.20(15)	1.40(0)	17.46(15)	0.52(1)				35	
	sartorite 1b	9	8.37(19)	1.26(7)	17.25(14)	0.52(1)				35	
LB93512	rathite	6	10.00(3)	0.20(1)	15.66(7)	0.24(2)	1.63(3)		0.04(0)	35	
	sartorite 2a	9	9.45(8)	0.46(3)	16.77(12)	0.27(2)				35	
	sartorite 2b	7	9.32(14)	0.61(6)	16.95(13)	0.27(2)				35	
	sartorite 2c	6	9.30(25)	0.71(14)	17.19(10)	0.29(5)				35	
A.E.	Sartorite	20	9.10	0.90	17.08					35	

Mineral	analytical formula			simplified:	data source		virtual *N*
seligmannite	$(Pb_{0.98}Tl_{0.01})_{\Sigma=0.99}$	$Cu_{1.01}$	$(As_{0.94}Sb_{0.06})_{\Sigma=1.00}$	$S_{3.00}$	$PbCuAsS_3$	EMP	
hatchite	$Pb_{0.98}Tl_{1.00}$	$(Ag_{0.87}Cu_{0.11})_{\Sigma=0.98}$	$(As_{1.97}Sb_{0.08})_{\Sigma=2.05}$	$S_{4.99}$	$PbTlAgAs_2S_5$	EMP	
rathite	$(Pb_{11.43}Tl_{0.23})_{\Sigma=11.66}$	$(Ag_{1.86}Fe_{0.04})_{\Sigma=1.90}$	$(As_{17.90}Sb_{0.28})_{\Sigma=18.18}$	S_{40}		EMP	
sartorite 1a	$(Pb_{8.20}Tl_{1.40})_{\Sigma=9.60}$		$(As_{17.46}Sb_{0.52})_{\Sigma=17.98}$	S_{35}		EMP	3.327
sartorite 1b	$(Pb_{8.37}Tl_{1.26})_{\Sigma=9.63}$		$(As_{17.25}Sb_{0.52})_{\Sigma=17.77}$	S_{35}		EMP	3.312
sartorite 2a	$(Pb_{9.45}Tl_{0.46})_{\Sigma=9.91}$		$(As_{16.77}Sb_{0.27})_{\Sigma=17.04}$	S_{35}		EMP	3.251
sartorite 2b	$(Pb_{9.32}Tl_{0.61})_{\Sigma=9.93}$		$(As_{16.95}Sb_{0.27})_{\Sigma=17.22}$	S_{35}		EMP	3.269
sartorite 2c	$(Pb_{9.32}Tl_{0.71})_{\Sigma=10.04}$		$(As_{17.19}Sb_{0.29})_{\Sigma=17.48}$	S_{35}		EMP	3.281
sartorite	$(Pb_{8.0}Tl_{1.5})_{\Sigma=9.5}$		$As_{17.5}$	S_{35}	$Pb_8Tl_{1.5}As_{17.5}S_{35}$	SC-XRD	3.375
sartorite	Pb_9		As_{18}	S_{36}	$Pb_9As_{18}S_{36}$	substr. ×9	3.000
"Mineral A"	$(Pb_{9.99}Tl_{0.14})_{\Sigma=10.13}$		$(As_{16.60}Sb_{0.30})_{\Sigma=16.90}$	S_{35}		84/1*	3.226
"Mineral A"	$(Pb_{9.64}Tl_{0.52})_{\Sigma=10.16}$		$(As_{16.96}Sb_{0.32})_{\Sigma=17.28}$	S_{35}		35/1*	3.274
Red sartorite	$(Pb_{9.10}Tl_{0.90})_{\Sigma=10.00}$		$As_{17.08}$	S_{35}		A.E. †	3.347

Notes: The formulae of sartorites 2a–2c were arbitrarily normalized to 35 S atoms (based on the present structure refinement). However, other superstructures may have different numbers of S atoms (smaller than, or equal to, 36).
N.A. = number of analyses; A.E. = analyses by A. Edenharter; SC-XRD = single crystal X-ray diffraction; substr. = substructure.
* Analyses of Laroussi et al. (1989).
† Analyses performed by A. Edenharter and obtained by courtesy of S. Graeser.

TABLE 3. Data collection and refinement parameters for sartorite

Diffractometer	Siemens CCD system
X-ray radiation	fine focus sealed tube, Mo$K\alpha$
X-ray power	50 kV, 40 mA
Temperature	293 K
Detector to sample distance	5.439 cm
Maximum 2θ	55.90°
Resolution	0.75 Å
Rotation width	0.3°
Frame size	512 × 512 pixels
Measuring time per frame	120 seconds
Measured reflections	53491
Index range	$-49 \le h \le 49$; $-10 \le k \le 10$; $-23 \le l \le 26$
Unique reflections	13085
Reflections > 2σ(*I*)	6293
R_{INT}	7.41%
R_σ	9.14%
Number of l.s. parameters	579
GooF	0.891
R_1, $F_o > 4\ \sigma(F_o)$	6.08%
R_1, all data	13.09%
wR_2 (on F_o^2)	14.40%
$R_{INT} = \Sigma \lvert F_o^2 - F_o^2(\text{mean}) \rvert / \Sigma F_o^2$	
$R_\sigma = \Sigma \sigma(F_o^2) / \Sigma F_o^2$	
$R_1 = \Sigma \lvert\lvert F_o \rvert - \lvert F_c \rvert\rvert / \Sigma \lvert F_o \rvert$	
$wR_2 = \{(\Sigma\ w[F_o^2 - F_c^2]^2 / \Sigma\ w[F_o^2]^2)\}^{1/2}$	
Goof = $\{(\Sigma\ w[F_o^2 - F_c^2] / [n-p])\}^{1/2}$	
$w = 1 / (\sigma^2[F_o^2] + [0.0595 * P]^2)$	
$P = (\max(F_o^2, 0) + 2\ F_c^2) / 3$	

RESULTS AND DISCUSSION

Unit-cell dimensions

The subcell dimensions of sartorite reported in literature are fairly consistent and describe an orthorhombic unit with the lattice constants listed in Table 1. Superstructure formation has been described by supercells with multiples of subcell *a* and *c*. The symmetry of the supercell is monoclinic, compared to the orthorhombic subcell, but in a number of determinations β = 90° was used. In their attempt to determine the true structure of sartorite, Ozawa and Takéuchi (1993) distinguished between "orthosartorite" and "clinosartorite." For the latter they defined a "new" subcell with lattice constants *a* = 20.06, *b* = 7.89, *c* = 4.19 Å, β = 102.1°, and space group $P2_1/c$ (Table 2). It is most interesting to see that the unit-cell parameters of the sartorite sample studied here are an integral multiple of the "clinosartorite" subcell, or, in other words, our subcell derived from the supercell is the same as that given by Ozawa and Takéuchi (1993) for "clinosartorite." Pring et al. (1993) reinterpreted the concept of "ortho-" and "clinosartorite," stating that satellite reflections occur along, or near, the [101]* direction and not along a* or c*, except when twinning is present. The apparent incompatibility of Pring et al.'s (1993) observation that structural modulations in sartorite occur along [101]*

TABLE 4. Site labels with element allocations, site occupancy factors (sof), fractional atomic coordinates, and equivalent isotropic displacement parameters for sartorite

Atom	type	sof	polyhedron type	*x*	*y*	*z*	U_{iso} (Å^2)
Pb1	Pb		*Z*	0.11812(2)	0.06199(11)	0.31086(5)	0.0540(2)
Pb2	Pb		*Z*	0.23129(2)	0.08379(12)	0.31078(6)	0.0599(3)
Pb3	Pb		*Z*	0.34273(2)	–0.59717(11)	–0.18503(5)	0.0514(2)
Pb4	Pb		*Z*	0.45338(2)	0.09418(11)	0.31461(5)	0.0568(3)
Pb5	Pb		*Z*	0.43835(2)	0.64077(11)	0.18296(5)	0.0533(2)
Pb6	Pb		*Z*	0.33030(2)	–0.40497(10)	0.20582(5)	0.0488(2)
Pb7	Pb		*Z*	0.21828(2)	–0.41642(12)	0.20383(6)	0.0613(3)
Pb8	Pb		*Z*	–0.10761(2)	0.07053(11)	0.29305(5)	0.0553(2)
Pb9	Pb		*Z*	0.00536(2)	0.07666(11)	0.29546(5)	0.0533(2)
As1	As		*B*3	0.14473(5)	-0.1612(3)	0.50326(11)	0.0409(5)
As2	As		*A*3	–0.14122(5)	0.4970(2)	0.37925(11)	0.0383(5)
As3	As		*B*3	0.23534(5)	–0.1793(3)	0.48906(11)	0.0439(5)
As4	As		*A*3	0.26684(5)	–0.0059(2)	0.13459(11)	0.0415(5)
M5a	Pb	0.318(5)	*B*3	0.36331(9)	–0.2758(5)	–0.0178(2)	0.0407(10)
M5b	As	0.682(5)	*B*3	0.36549(12)	–0.3088(6)	-0.0044(3)	0.0486(15)
As6	As		*A*3	0.36103(6)	0.0221(3)	0.11955(11)	0.0454(5)
As7	As		*B*3	0.46747(5)	0.7081(3)	0.01033(12)	0.0481(5)
As8	As		*A*3	0.49761(5)	0.0354(2)	0.13258(11)	0.0421(5)
As9a	As	0.67(4)	*B*3	0.4085(5)	–0.7093(15)	0.0103(5)	0.057(3)
As9b	As	0.33(4)	*B*3	0.4224(3)	–0.6619(18)	0.0197(4)	0.022(3)
As10	As		*A*3	0.40337(5)	0.5095(3)	0.36345(11)	0.0421(5)
As11	As		*B*3	0.30861(5)	0.1850(2)	0.49187(10)	0.0378(5)
As12	As		*A*3	0.28781(8)	0.5218(3)	0.38204(13)	0.0678(8)
M13a	Pb	0.218(5)	*B*3	0.19864(17)	0.2524(8)	0.5261(3)	0.0376(16)
M13b	As	0.782(5)	*B*3	0.20500(14)	0.1935(6)	0.5417(3)	0.0515(13)
As14	As		*A*3	0.18075(5)	0.4819(3)	0.36831(11)	0.0391(5)
As15	As		*B*3	0.07986(5)	0.1697(3)	0.49597(11)	0.0440(5)
As16	As		*A*3	0.07553(6)	0.4960(2)	0.38595(11)	0.0485(6)
As17	As		*B*3	0.01729(6)	–0.1830(3)	0.47361(12)	0.0542(6)
As18	As		*A*3	0.04364(5)	–0.0260(2)	0.13245(10)	0.0367(5)
S1	S			0.05914(12)	0.3548(6)	0.2860(3)	0.0369(11)
S2	S			0.06506(15)	–0.0469(6)	0.4188(3)	0.0513(14)
S3	S			–0.10464(12)	0.2996(6)	0.4432(3)	0.0413(12)
S4	S			0.09407(12)	0.1477(6)	0.1533(3)	0.0364(11)
S5	S			0.17148(13)	0.3363(6)	0.2698(3)	0.0446(13)
S6	S			0.19372(13)	0.0068(6)	0.4287(3)	0.0415(12)
S7	S			0.19347(13)	–0.3325(7)	0.5384(3)	0.0495(14)
S8	S			0.22449(13)	0.1691(6)	0.1605(3)	0.0440(12)
S9	S			0.28301(13)	0.3747(6)	0.2853(3)	0.0378(11)
S10	S			0.30124(14)	–0.0384(6)	0.4208(3)	0.0483(13)
S11	S			0.32402(17)	–0.1802(7)	0.0648(3)	0.0640(17)
S12	S			0.31640(13)	0.1724(6)	0.1581(3)	0.0404(12)
S13	S			0.39195(13)	0.3540(6)	0.2686(3)	0.0462(13)
S14	S			0.40903(13)	–0.5148(6)	–0.0741(3)	0.0431(12)
S15	S			0.42766(15)	0.8592(6)	0.0598(3)	0.0519(14)
S16	S			0.49967(15)	0.8788(7)	0.2270(3)	0.0504(14)
S17	S			0.47646(14)	0.4724(6)	0.0782(3)	0.0477(13)
S18	S			0.52090(13)	0.8488(6)	0.0661(3)	0.0444(12)
S19	S			0.55163(12)	0.1855(6)	0.1625(3)	0.0409(12)
S20	S			0.38472(13)	–0.1184(6)	0.2156(3)	0.0444(13)
S21	S			0.37864(12)	–0.5356(6)	0.0741(3)	0.0413(12)
S22	S			0.34784(13)	0.3424(6)	0.4425(3)	0.0436(12)
S23	S			0.35571(13)	0.6851(6)	0.3407(3)	0.0426(12)
S24	S			0.27767(12)	–0.1522(6)	0.2326(3)	0.0402(12)
S25	S			0.25394(12)	0.0133(6)	0.5763(3)	0.0378(11)
S26	S			0.25844(12)	0.3409(6)	0.4415(3)	0.0427(12)
S27	S			0.22385(12)	0.6686(6)	0.3448(3)	0.0388(11)
S28	S			–0.16240(12)	0.3520(6)	0.2827(3)	0.0397(12)
S29	S			0.15915(13)	0.0510(6)	0.5842(3)	0.0440(12)
S30	S			0.11955(13)	0.3154(7)	0.4432(3)	0.0439(12)
S31	S			–0.13158(13)	0.1553(6)	0.1522(3)	0.0400(11)
S32	S			–0.05376(12)	0.3321(6)	0.2670(3)	0.0398(12)
S33	S			–0.02922(12)	–0.0020(6)	0.4273(2)	0.0363(11)
S34	S			0.03377(14)	0.3475(7)	0.4558(4)	0.068(2)
S35	S			0.00347(12)	0.1617(6)	0.1550(2)	0.0365(11)

TABLE 5. Selected interatomic M-S distances (Å) for the $MS_{9(/8)}$ and $MS_{7(/6)}$ coordination polyhedra in sartorite

Pb1		Pb6		As2		As6		As10		As14	
S32	3.172(5)	S23	2.775(6)	S28	2.252(6)	S20	2.245(6)	S13	2.234(6)	S5	2.254(6)
S1	3.175(5)	S24	2.943(5)	S3	2.291(5)	S11	2.253(6)	S23	2.241(5)	S31	2.273(5)
S5	3.180(5)	S20	3.034(5)	S4	2.343(6)	S12	2.321(6)	S19	2.335(6)	S27	2.315(6)
S4	3.182(6)	S13	3.066(5)	S7	3.109(6)	S15	3.266(7)	S22	3.168(6)	S26	3.193(5)
S28	3.222(6)	S9	3.154(6)	S8	3.362(5)	S22	3.651(6)	S18	3.177(5)	S30	3.281(6)
S31	3.312(5)	S11	3.312(6)	S29	3.735(5)	S21	3.706(6)	S15	4.000(6)	S7	3.660(6)
S30	3.321(6)	S12	3.483(5)	S30	3.794(6)			S14	4.176(6)	S6	4.319(6)
S6	3.335(5)	S25	3.562(5)								
S2	3.355(6)	S21	3.662(6)								
Pb2		Pb7		As3		As7		As11		As15	
S5	2.995(5)	S27	2.878(6)	S6	2.303(5)	S17	2.291(6)	S10	2.251(6)	S34	2.250(6)
S8	3.054(6)	S24	3.028(5)	S25	2.318(6)	S15	2.300(6)	S26	2.308(5)	S2	2.299(6)
S6	3.065(6)	S28	3.041(5)	S7	2.365(6)	S18	2.369(5)	S22	2.309(6)	S30	2.313(6)
S9	3.124(5)	S29	3.108(5)	S27	3.086(6)	S14	3.047(5)	S21	3.047(5)	S33	3.001(5)
S24	3.185(6)	S5	3.108(6)	S10	3.274(6)	S17	3.352(6)	S25	3.229(6)	S29	3.281(5)
S10	3.218(5)	S9	3.115(5)	S11	3.552(6)	S19	3.501(6)	S12	3.481(6)	S4	3.416(6)
S26	3.311(6)	S25	3.225(6)	S26	4.047(6)	S18	3.883(6)	S11	4.175(6)	S3	4.412(6)
S27	3.373(5)	S8	3.408(5)								
S28	3.407(5)	S7	3.809(6)								
Pb3		Pb8		As4		As8		As12		As16	
S13	3.025(5)	S31	2.867(6)	S24	2.247(6)	S16	2.254(6)	S9	2.240(6)	S1	2.269(6)
S14	3.055(5)	S28	3.013(5)	S8	2.254(6)	S18	2.284(6)	S26	2.291(6)	S30	2.307(5)
S10	3.083(6)	S32	3.018(5)	S12	2.309(5)	S19	2.326(5)	S27	2.641(5)	S34	2.598(7)
S9	3.110(5)	S5	3.091(5)	S11	3.126(7)	S15	3.071(5)	S22	2.733(5)	S31	2.704(6)
S12	3.160(6)	S1	3.159(6)	S7	3.287(5)	S17	3.658(5)	S22	3.130(6)	S35	3.201(5)
S22	3.187(6)	S3	3.501(6)	S26	4.045(6)	S18	4.015(6)	S10	3.573(5)	S2	3.706(5)
S20	3.273(6)	S4	3.514(5)	S25	4.063(5)			S11	3.853(6)	S3	3.748(6)
S24	3.310(5)	S29	3.575(6)								
S23	3.316(5)	S33	3.611(4)								
Pb4		Pb9		M5a		As9a		M13a		As17	
S16	3.083(6)	S35	2.889(4)	S11	2.559(8)	S14	2.292(13)	S29	2.615(9)	S33	2.304(5)
S13	3.089(5)	S32	2.973(5)	S21	2.741(7)	S21	2.323(16)	S6	2.735(8)	S33	2.436(5)
S14	3.123(6)	S1	3.023(5)	S15	2.808(6)	S22	2.627(16)	S8	2.746(8)	S2	2.538(7)
S18	3.126(5)	S32	3.097(5)	S10	2.821(6)	S17	3.006(16)	S25	2.839(8)	S35	2.822(5)
S17	3.194(5)	S2	3.139(5)	S23	2.890(7)	S18	3.516(18)	S30	3.139(8)	S34	2.923(7)
S16	3.213(6)	S1	3.165(5)	S14	2.937(7)	S15	3.582(13)	S26	3.172(9)	S3	3.494(5)
S19	3.271(5)	S33	3.248(5)	S22	3.536(6)			S7	3.297(9)	S34	3.789(6)
S20	3.368(5)	S35	3.462(5)								
		S34	3.832(7)								
Pb5		As1		M5b		As9b		M13b		As18	
S20	2.948(5)	S7	2.273(5)	S21	2.371(7)	S14	2.183(11)	S25	2.320(7)	S35	2.232(5)
S16	2.969(6)	S3	2.306(6)	S11	2.514(9)	S21	2.380(13)	S29	2.367(8)	S32	2.273(6)
S15	2.976(6)	S29	2.321(6)	S15	2.769(7)	S17	2.381(12)	S8	2.587(8)	S4	2.312(5)
S19	3.072(6)	S6	2.928(6)	S10	2.842(7)	S22	3.246(12)	S6	2.668(8)	S34	3.243(6)
S17	3.087(6)	S2	3.257(6)	S14	2.875(8)	S18	3.356(13)	S26	3.341(8)	S3	3.310(6)
S21	3.123(5)	S31	3.387(6)	S23	3.211(8)	S15	3.864(15)	S30	3.547(7)	S34	3.767(8)
S16	3.356(5)	S30	4.356(6)	S22	3.854(7)			S7	3.768(7)	S33	4.312(5)
S13	3.523(6)										

and our finding of a sartorite superstructure with $a' = 9c$ (Table 1) can easily be explained by the fact that Pring et al. (1993, their Fig. 4) indexed their electron diffraction pattern using the orthorhombic subcell of Nowacki et al. (1961). With the choice of a different (monoclinic) subcell the modulation of the sartorite structure of Pring et al. (1993) occurs along a principal axis in reciprocal space. From geometry, $\beta = 90° + \tan^{-1}(4.19/19.62) = 102.05°$ for this monoclinic subcell (Table 1). Pring et al. (1993) suggested that sartorite generally has an incommensurate lattice. In this respect the superstructure described here can be regarded as a so-called "lock-in phase" with a composition that yields a commensurate lattice.

Cation substitution

The unit-cell contents of pure ideal sartorite ($PbAs_2S_4$, $Z = 4$) are $Pb_4As_8S_{16}$. Accordingly, the unit-cell contents of the ninefold superstructure described here would be $Pb_{36}As_{72}S_{144}$. However, the refined unit-cell content is $Pb_{38.14}As_{69.86}S_{140}$ (simplified $Pb_{38}As_{70}S_{140}$), having about 2 Pb more and about 2 As less than expected, and yielding a total excess of 5.86 (simplified 6) positive charges. Notice that the latter formula is not charge balanced because our diffraction experiment does not allow discrimination between isoelectronic Pb^{2+} and Tl^{+}. As can be seen from the chemical analyses in Table 2, the sartorite samples contain variable and significant amounts of Tl but they are devoid of Ag, the other substituting element common in sartorite homologues which contain $N = 4$ slabs. Charge balance in the structurally investigated sartorite is achieved by two substitutions: mechanism (1) reduces the total number of As atoms from 72 to 70 and increases the total number of Pb atoms from 36 to 38; mechanism (2) replaces 6 Pb atoms with Tl. These substitutions can be coupled and shortened into (3):

TABLE 6. Estimated bond valences (BE) and selected polyhedral parameters for individual coordination polyhedra in the sartorite superstructure

Atom	CN	BVE	V_p	V_s	v	ECC_v	SPH_v
Pb1	9	1.382	69.338	144.128	0.0168	0.1057	0.9747
Pb2	9	1.696	65.209	135.879	0.0192	0.1255	0.8886
Pb3	9	1.756	63.754	132.492	0.0166	0.1211	0.9308
Pb4	8	1.487	55.214	134.897	0.0215	0.1155	0.9503
Pb5	8	1.856	53.715	128.728	0.0024	0.2730	0.9154
Pb6	9	1.926	67.183	138.886	0.0114	0.3782	0.9377
Pb7	9	1.905	63.811	135.305	0.0362	0.2704	0.8124
Pb8	9	1.687	69.391	144.441	0.0182	0.3646	0.9660
Pb9	9	1.886	64.110	136.239	0.0383	0.2803	0.8002
As1	7	2.980	35.985	104.281	0.0881	0.7236	0.5259
As2	7	2.927	35.690	104.454	0.0971	0.7413	0.8833
As3	7	2.708	37.585	108.395	0.0837	0.7286	0.8337
As4	7	3.102	37.393	111.500	0.1138	0.7667	0.6241
Pb5a	7	3.371	36.291	103.180	0.0705	0.3227	0.7710
As5b	7	1.984	36.291	103.179	0.0705	0.5699	0.7710
As6	6	3.018	27.586	105.518	0.1787	0.7393	0.9519
As7	7	2.781	36.712	104.442	0.0711	0.6898	0.7383
As8	6	2.933	26.678	106.969	0.2165	0.7636	0.7768
As9a	6	2.326	28.784	106.644	0.1521	0.6394	0.9366
As9b	6	2.810	28.784	106.644	0.1521	0.7172	0.9366
As10	7	3.127	37.140	112.222	0.1254	0.7723	0.6015
As11	7	3.014	36.533	105.147	0.0818	0.7251	0.6259
As12	7	2.748	34.984	101.827	0.0921	0.6908	0.8534
Pb13a	7	3.015	36.535	110.052	0.1227	0.3522	0.9094
As13b	7	2.446	36.535	110.052	0.1227	0.6901	0.9094
As14	7	3.014	36.018	108.807	0.1252	0.7386	0.4976
As15	7	3.039	36.436	106.364	0.0947	0.7389	0.5142
As16	7	2.676	34.733	102.225	0.1021	0.6929	0.8590
As17	7	2.418	35.232	104.892	0.1124	0.6563	0.8868
As18	7	3.063	36.773	110.018	0.1167	0.7485	0.5015

Notes: CN = coordination number; BVE = bond valence estimation; V_p (Å^3) = polyhedral volume; V_s (Å^3) = volume of sphere least-square fitted to polyhedron with radius r_s and standard deviation $\sigma(r_s)$; v (%) volume distortion = 100 ($V_i - V_p$) / V_i where V_i is the ideal and V_p the real polyhedron volume. See Makovicky and Balić-Žunić (1998) for details on V_i; ECC_v volume eccentricity = $1 - [(r_s - \Delta) / r_s]^3$ where Δ = distance between centroid and central atom; SPH_v = volume sphericity = $1 - 3\sigma(r_s) / r_s$.

$$2\ Pb^{2+} \rightarrow 2\ As^{3+} + S^{2-} \quad (1)$$

$$6\ Tl^{+} \rightarrow 6\ Pb^{2+} + 3S^{2-} \quad (2)$$

$$2\ Pb^{2+} + 6\ Tl^{+} \rightarrow 2\ As^{3+} + 6\ Pb^{2+} + 4\ S^{2-} \quad (1) + (2)$$

$$6\ Tl^{+} \rightarrow 2\ As^{3+} + 4\ PbS \quad (3)$$

This substitution not only includes cations but also affects sulfur. In total 4 Pb and 2 As are replaced by 6 Tl, with a concurrent loss of 4 S, and the corresponding structurally refined (simplified) formula (cell content/*Z*) is $Pb_8Tl_{1.5}As_{17.5}S_{35}$. This compares well with the empirical formula $Pb_{8.2}Tl_{1.4}As_{17.5}Sb_{0.5}S_{35}$ derived from the EMP analyses (cf., sartorite 1a, Table 2). Small amounts of Sb substitute for As but could not be located in the present structure refinement. The involvement of sulfur in the substitution schemes listed above contrasts with the known mechanisms, recently reformulated for rathite, where the substitution $Ag^{+} + As^{3+} \rightarrow 2\ Pb^{2+}$ seems to be essential compared to the apparently optional substitution $Tl^{+} + As^{3+} \rightarrow 2\ Pb^{2+}$ (Berlepsch et al. 2002), and where the number of sulfur atoms does not change with cation substitution.

Our data can be compared with previously published analyses. Significant deficiency in As compared to the conventionally accepted chemical formula $PbAs_2S_4$ has also been reported by Ozawa (1993). Minor Tl in sartorite has been reported by Nowacki and Bahezre (1963) as well as by Ozawa (1993). Significant amounts of Tl, exceeding 4 wt%, were measured by Laroussi et al. (1989). Similar amounts of Tl were found in a

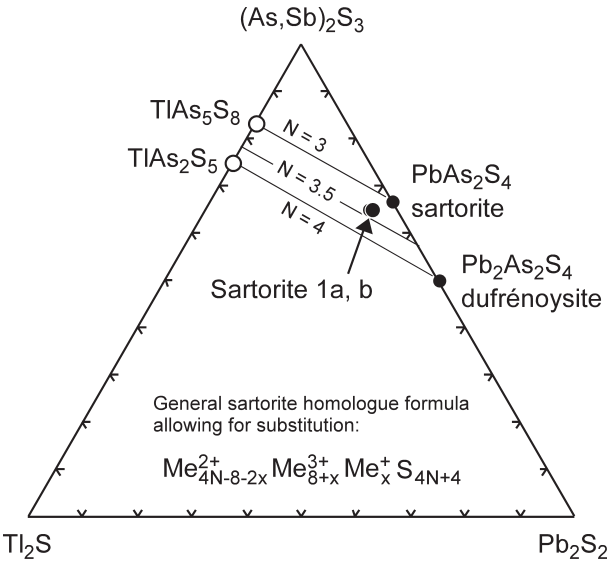

FIGURE 2. Selected known and hypothetical members $N = 3$ and $N = 4$, respectively, of the sartorite homologous series in the phase triangle Pb_2S_2 – $(As,Sb)_2S_3$ – (Ag_2S and Tl_2S). Solid circles indicate known phases, empty circles hypothetical end members. $PbAs_2S_4$ is the ideal sartorite composition, generally accepted in literature. Three isopleths of equal *N* values and the sartorite 1 data from Table 2 are added.

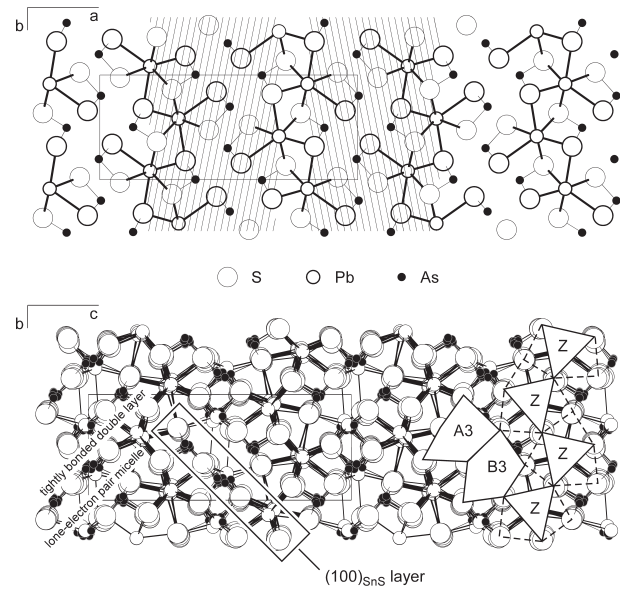

FIGURE 3. The crystal structure of sartorite: projections of (above) the substructure (Iitaka and Nowacki 1961) along [001] and of (below) the superstructure along [100]. The SnS-based slices $(301)_{SnS}$ and $(30\bar{1})_{SnS}$ are indicated by ruling (above). The polyhedral labeling scheme for sartorite homologues, according to Berlepsch et al. (2001), is indicated and a $(100)_{SnS}$ layer, as displayed in Figure 5 in view normal to the plane, is outlined (below).

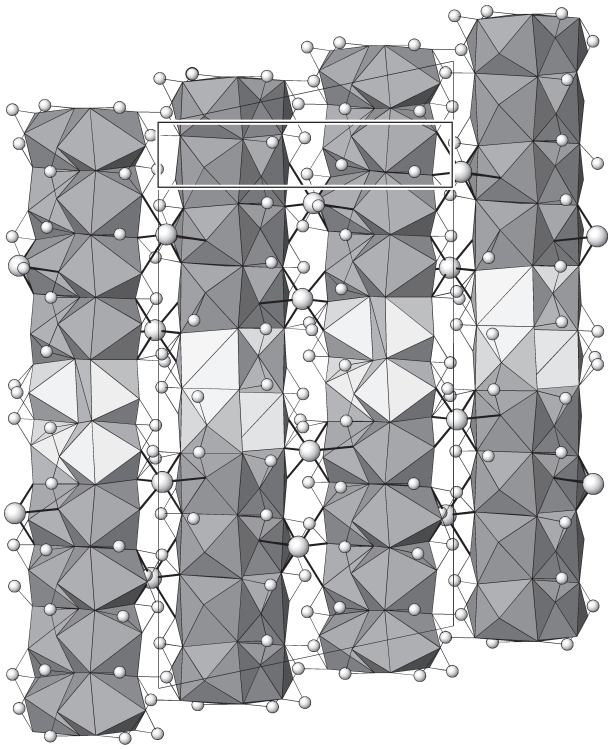

FIGURE 4. Semi-polyhedral view of the sartorite superstructure along [010]. The polyhedral "columns" are projections of zigzag (100) layers of Pb trigonal coordination prisms (*Z* in Fig. 3). Light gray polyhedra have coordination number 8 (CN8; the missing cap is easily visible); dark gray polyhedra have CN9. Large and small spheres indicate (Pb, Tl) and As, respectively, situated in the SnS-like slabs. The orthorhombic sartorite subcell of Nowacki et al. (1961) is indicated.

"red" sartorite sample originating from the new Lengenbach quarry (Graeser in Hofmann et al. 1993). It should be noted that Edenharter (S. Graeser, pers. comm.) observed substitution of both Pb and As by Tl. As shown in Table 2, Tl concentrations in sartorite can be as high as 6.5 wt% (this study).

The cation ratios due to S vacancy are analogous to those connected with the increase of the homologue order *N*. Therefore, they can be evaluated by means of "virtual *N*," calculated from the general formula of the sartorite homologous series: $Me^{2+}_{4N-8-2x}Me^{3+}_{8+x}Me^{+}_{x}S_{4N+4}$. Using the substitution mechanism $2x\ Me^{2+} \leftrightarrow Me^{3+}_{x} + Me^{+}_{x}$, this yields $N = [2\ (Me^{2+} + 2\ Me^{+})/(Me^{3+} - Me^{+})] + 2$. These calculations yield values of $N = 3.32$ to 3.33 for sartorite 1, and 3.25 to 3.28 for sartorite 2 in Table 2. However, both have the $N = 3$ substructure, i.e., the deviations are fully ascribed to the substitution schemes involving S.

The analyses of "mineral A" of Laroussi et al. (1989) resemble those of our sartorite samples and are given in Table 2 for comparison. Laroussi et al. (1989) calculate for this "mineral A" a homologue order of $N = 3.33$, intermediate between sartorite ($N = 3$) and dufrénoysite ($N = 4$), and state that no such sartorite homologue is known (Fig. 2). They tried to explain the situation with a small-scale intergrowth of chabournéite and sartorite, although a combinatorial model with $N_{1\text{-}3} = 3,3,4$ would yield a simpler explanation. Our calculations of virtual *N* indicate $N = 3.23$ to 3.27 for the data of Laroussi et al. (1989). Due to the above described substitutions, the data points are shifted away from the isopleth with $N = 3$ toward a higher *N* value (Fig. 2). Pure (Tl, Ag) + As ↔ 2 Pb substitution, not affecting S, e.g., as in rathite, would not have this effect but would shift the data points along the corresponding isopleth with constant *N*. Obviously, "mineral A" of Laroussi et al. (1989) is sartorite as well.

The role of "large" monovalent cations

Considering the importance of Tl^{+} and Ag^{+} substitution for sartorite and rathite and baumhauerite polytypes, respectively, we note that most of the natural sartorite homologues studied in the past occur only at the type locality (Lengenbach, Binntal, Ct. Valais, Switzerland). This dolomite hosted Fe-Zn ore deposit is enriched in Tl-As-(Sb) and significant variations of the bulk rock chemistry are observed on a meter scale (e.g., Hofmann et al. 1993; Hofmann and Knill 1996). Minerals originating from the new mine (opened in 1988), topologically situated about 30 m above the old mine (closed in 1987), are characterized by high contents of Tl, As, and Sb compared to the material from the old mine. This fact is reflected in the various new Tl-sulfosalts from Lengenbach reported in the past 15 years (e.g., edenharterite, jentschite, erniggliite, stalderite, bernardite, sicherite). Knowing this, it is understandable why the above mentioned importance of Tl and Ag becomes much more pronounced in recently found material originating from the new mine, e.g., baumhauerite-2*a* and baumhauerite-ψ*O*3*abc* (Pring and Graeser 1994), rathite (Berlepsch et al. 2002), and sartorite (this study).

The substructure of sartorite

The substructure of sartorite is shown in Figure 3; some structural aspects have been marked. Zigzag walls composed of columns of "standing" tricapped trigonal coordination prisms of Pb (CN9) alternate with slabs composed of "lying" monocapped trigonal coordination prisms of As and Pb (CN 7); these slabs are based on the SnS-archetype. The substructure of sartorite is visualized as being composed of slices of SnS-like structure cut parallel to the $(301)_{SnS}$ and $(30\overline{1})_{SnS}$ planes (Fig. 3, top). Note that these slices include polyhedra from both the walls and the slab and that they are $N = 3$ polyhedra thick.

According to the labeling scheme for coordination polyhedra in sartorite homologues introduced by Berlepsch et al. (2001) *Z* denotes "standing" tricapped trigonal coordination prisms in the zigzag walls whereas *AN*, *BN*, and *CN* denote "lying" monocapped trigonal coordination prisms within the slabs (with $N = 3$ or 4). Sartorite is an $N_{1,2} = 3,3$ member of the sartorite homologous series (Fig. 3, below) with *Z* hosting Pb and *A*4/*B*4 hosting As and Pb (details are discussed below). Other $N_{1,2} = 3,3$ sartorite homologues are twinnite $Pb(Sb,As)_2S_4$ (Jambor 1967; not observed in the Lengenbach deposit), and synthetic $BaSb_2Se_4$ (Cordier and Schäfer 1979) and $BaSb_2S_4$ (Cordier et al. 1984).

The ninefold superstructure of sartorite

The projections in Figure 3 show that the studied structure is an $N_{1,2} = 3,3$ sartorite homologue. A semi-polyhedral view of

the sartorite superstructure along [010] is shown in Figure 4. However, the differences between the (average) substructure (Iitaka and Nowacki 1961) and the superstructure are not noticeable in this view. They can be best appreciated when looking at the projections perpendicular to the $(100)_{SnS}$ type layers (Fig. 5). Iitaka and Nowacki (1961) mentioned that the infinite S-As-S chains along [001] in the sartorite substructure cannot exist due to the misfit in size between PbS_9 and AsS_7 coordination polyhedra and the resulting unusually long As-S distances. The importance of the so-called crankshaft chains as a feature that allows an ideal adjustment to the requirements of the various large cations (e.g., Pb, Tl, Ba) incorporated in the crystal structures of the sartorite homologues *sensu largo* was pointed out by Makovicky (1985).

In Figure 5 the idealized $(100)_{SnS}$ type layers of the sartorite substructure (left, subcell × 9) are compared with the experimentally derived layers from the superstructure (right). The dashed lines in Figure 5 indicate the arrangement of S atoms around the cations in the $(100)_{SnS}$ layers. This arrangement is purely rectangular in the substructure but is trapezoidal in the real structure, especially for the S coordination around As. In case of *Z*-type cations (Pb/Tl) this arrangement tends toward rectangular (e.g., S around Pb3 in Fig. 5). Inside the trapezoids the As atoms are bound to S ligands via short bonds either in a "sideways" (e.g., As1 and As4) or in a "top/bottom" (e.g., As2 and As3) manner. In this way the crankshaft chains are formed; they are drawn with bold lines in Figure 5. All known sartorite homologues *sensu largo* are two coordination polyhedra "thick," i.e., they have one lattice parameter of about 8.4 Å in common. In contrast, the superstructure described here is nine polyhedra "thick," the $(100)_{SnS}$ layer in Figure 5 shows why.

The 9*c* modular array (periodicity of the superstructure along *a*) is composed of five complete or fragmented crankshaft chains, oriented in two different directions, perpendicular to each other. The array contains two approximate mirror planes perpendicular to *a*, at the level of S13-S14-S15 and As14-M13b-Pb7, respectively. The former one projects the crankshaft chain As4-As6-M5b into As7-As8-As10 and As18-As2-As1-As3 into As14-As12-As11-As9a. The latter projects a fragmented "chain" As14-As16-As15-As17 into a similar one, As14-As12-As11-As9a, and the As18-As2-As1-As3 chain into As10-As8-As7-M5b. The fragmentary character of two chains that tentatively start from As14, stems from a statistical combination of a typical crankshaft configuration with another configuration that consists of separate As_2S_4 groups (As15-As16 and As11-As12) combined with isolated AsS_3 units (As9b, M13b, As14, As18). This is caused by the splitting of the As9, As12, As16, and As17 positions into two competing configurations (described in detail below). Both reflection operations, and the fragmentation, are apparently connected with the statistical occupation of the M5 and M13 positions. The distribution of (statistical) As_2S_4 groups vs. well defined crankshaft chains in the 9*c* column leads to another type of division: the former configuration occurs in a stack of five subcells parallel to **a**, from As9 to As17, the latter in the stack of remaining four subcells, from As1 to As7. The former stack is similar to configurations in similar Ba-Sb sulfosalts (e.g., $BaSb_2S_4$; Cordier et al. 1984), the latter is similar to configurations observed in

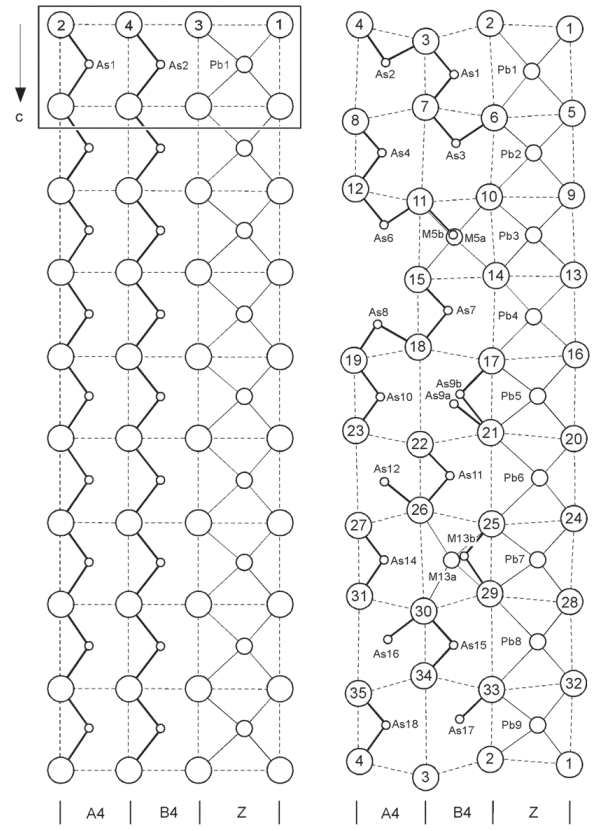

FIGURE 5. $(100)_{SnS}$ type layers in the sartorite substructure (left, ×9) and in the superstructure (right). The dashed fine lines indicate the arrangements of S atoms: rectangular in the substructure vs. trapezoidal in the superstructure. Short As-S bonds (bold lines) form finite, diagonally oriented crankshaft chains in the real structure whereas they average to the infinite (and non-existing) S-As-S chains in the substructure. Half way between S12 and S19 is the place of the missing S atom in this layer.

$N = 4$ sartorite homologues. The missing S position lies in the continuation of the S13 to S15 string of anions and the large lone-electron pair micelle contains electron pairs of As6, As8, and As9.

The crankshaft chains and intermediate space are underlain by similar elements on the other side of the tightly bonded SnS-like slab, i.e., the chains on the two sides are generally parallel. The respective mirror planes of the two faces of the SnS-like slabs project via symmetry centres. The two pseudo-mirror planes are not distributed evenly in the 9*c* array: instead they are 3.5 subcells and 5.5. subcells apart. In other words, they are separated by sets of two and three parallel crankshaft chains, respectively. Extension of the former set to 5.5 subcells (i.e., three parallel, partly fragmented crankshaft chains) apparently is the clue to the 11*c* superperiod observed by Iitaka and Nowacki (1961). Statistical mixture of sets of 3.5 and 5.5 subcells would then lead to a sartorite sample with an incommensurate superlattice.

Borrowing a term from the textile/basket industry, this "patterning" of SnS-like slabs can be called a *twill* pattern. Another

compound for which a similar twill pattern is developed is "senandorite" (andorite VI), ideally $PbAgSb_3S_6$ (Sawada et al. 1987). In this lillianite homologue $N = 4$, the sixfold sequence of 4 Å subcells has a distinct pattern of crankshaft chains As_3S_7, pairs As_2S_4, and marginal AsS_3 groups (Fig. 6). The twill pattern is based on one chain along one diagonal and a pair of parallel chains along the opposite diagonal leading one immediately to think of the fourfold structure of "quatrandorite" (andorite IV, Moëlo et al. 1984). Details of such derivations are in Moëlo et al. (1984). Distribution of arsenic configurations utilizes the entire four trapezoids broad $(100)_{PbS}$ strip and is closely connected with the distribution of silver in this strip.

The twill pattern in sartorite is based on crankshaft chains meeting on the pseudo-mirror planes (Fig. 5). The pattern in andorite is different, the crankshaft chains abutting head-to-tail sideways, in a *c*-glide scheme, broken only by a doubling of crankshaft chains in one direction. In "senandorite," only two configurational types of 4 Å tiers exist, in a regular, albeit not simply, periodic alternation. In sartorite there are four different types of 4 Å tiers in the 9*c* stacking sequence.

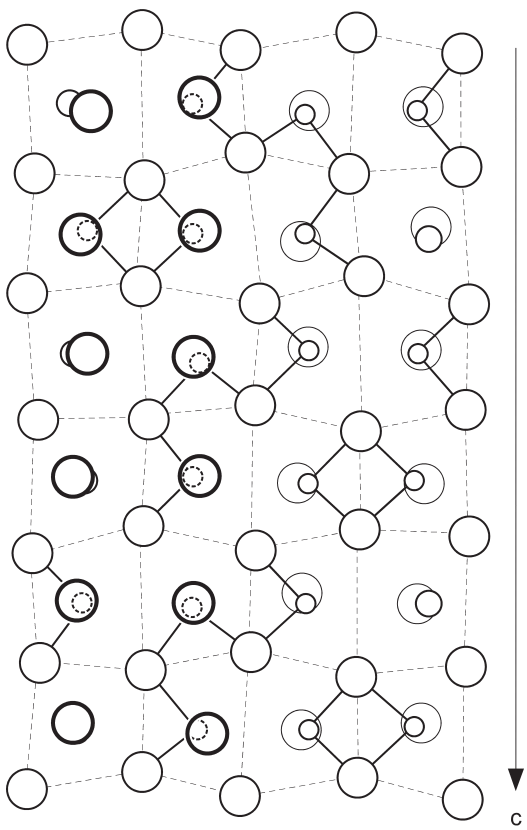

FIGURE 6. Twill pattern of crankshaft chains in "senandorite" (andorite VI), ideally $PbAgSb_3S_6$ (Sawada et al. 1987). The sixfold sequence of 4 Å subcells has a distinct pattern of crankshaft chains As_3S_7, pairs As_2S_4, and marginal AsS_3 groups. The twill pattern is based on one crankshaft chain along one diagonal and a pair of parallel crankshaft chains along the opposite diagonal. Circles in order of decreasing size represent: S, Pb, Ag, Sb.

Coordination polyhedra

Two different kinds of coordination polyhedra in sartorite homologues have been introduced above: the "standing" tricapped trigonal prisms with coordination number 9 (CN9) and the "lying" monocapped trigonal prisms with CN7 (= the SnS based coordination). Our refinement of the sartorite superstructure revealed several coordination polyhedra with CN6 and CN8. Due to the loss of one S atom pfu during element substitution (see above) As6, As8, and As9a,b have only six and Pb4 and Pb5 only eight S ligands [the use of CN9 (CN8) and CN7 (CN6) is related to the full coordination sphere around cations and does not contradict the fact that As and its three closest ligands form the "usual" trigonal AsS_3 pyramids]. Although isoelectronic Tl^+, Pb^{2+}, and Bi^{3+} cannot be distinguished with the X-ray diffraction set-up used here, it is possible to distinguish between them in the BV estimation approach, because the r_0 values (fitted bond valence constants) used in this procedure are almost identical ($r_0 = 2.543$ Å) for the three cations (Hummel and Armbruster 1987). Bond valence estimations according to Brown and Altermatt (1985), $BV = \Sigma \exp([r_0 - r_{ij}] / 0.37)$, where r_{ij} = individual metal to sulfur distance, revealed no direct link between CN8 and bond valence sums of about 1, indicative of a pure Tl^+ position. One cation (Pb1) with a low estimated BV of 1.38 (Table 6) has CN9. The Tl distribution over the other *Z*-type sites is believed to be random. Pb4 (CN8) has an intermediate estimated BV of 1.49 and the remaining *Z*-type cations yield BV values in the range 1.69–1.93 (Table 6). For the *A*3- and *B*3-type cations the BV estimates range from 2.42 (As17) to 3.13 (As10). The corresponding values for the split positions (M5a,b; As9a,b; M13a,b) are controversial due to unresolved S disorder around these positions. The somewhat low BV estimates of 2.42 (As17) and 2.67 (As16) can be explained with the help of the element specific bond-length hyperbolae (see below) as coming from unresolved split positions as well.

The CN8 polyhedral volumes (V_p) of 55.2 and 53.7 $Å^3$ for Pb4 and Pb5, respectively, obviously differ from those for CN9, which range from 63.2 to 69.3 $Å^3$ (Table 6). The latter values agree well with $V_p = 64.6 \pm 1.6$ $Å^3$ for Pb with CN9 in sartorite homologues given by Berlepsch et al. (2001). The somewhat higher V_p values for Pb1 and Pb8 are still significantly lower than the $V_p = 76.06 \pm 2.0$ $Å^3$ for Tl with CN9 in sartorite homologues (Berlepsch et al. 2001) and thus not indicative of predominantly Tl^+ positions. The situation for CN6 and CN7 is comparable (Table 6): the polyhedral volumes V_p for As with CN6 are significantly lower (26.7 to 28.8 $Å^3$) than those for As(/Pb) with CN7 (34.7 to 37.6 $Å^3$). Again, the latter values agree well with $V_p = 37.3 \pm 1.4$ $Å^3$ for As with CN7 in sartorite homologues given by Berlepsch et al. (2001).

The method of bond-length hyperbolae (Berlepsch et al. 2001) allows us to distinguish, with good reliability, between "true" relationships between different As-S (and other) bond lengths in a coordination polyhedron and the "apparent" bonding schemes from unresolved split cation and/or ligand positions. This concept [originally defined by Trömel (1981) for Sb^{3+}, Te^{4+}, and I^{5+} bonds with O atoms] is based on the fact that bond pairs $x_n y_n$ of opposing short and long bonds of a single coordination polyhedron of a given cation conform to the hy-

perbolic correlation $(x_n - a)(y_n - a) = c$ ($c > 0$). However, sometimes other bond pairs lying on a linear join (perpendicular to the line $y = x$) between the two branches of a hyperbola are observed. The latter set is interpreted as the result of superimposed and not fully resolved atomic positions indicating that the observed coordination is an average of at least two distinct situations. For the resolved split cation positions, deviations from the hyperbolic trend are due to the unresolved nature of the averaged ligand positions. Note that *Z*-type cations are not to be used in this approach because the bond pairs do not consist of opposing bonds, i.e., they are not defined.

Figure 7 shows the calculated hyperbolae for the sartorite homologues with the bond-pairs As-S and M-S for the sartorite superstructure (this study) added. Normal and manifestly split cation positions are referred to by filled circles and empty squares, respectively. As can be seen in Figure 7, most of the As-S bond-pairs lay on, or close to, the corresponding hyperbola, whereas the values for the split positions are displaced. As shown by Berlepsch et al. (2001) it is usual that at least one bond-pair formed by (unresolved) ligands around a split cation position is displaced significantly from the corresponding hyperbola (e.g., As5b, As9a, As13b). The positions of four bond-pairs (As12, As16, 2 × As17) on the above mentioned linear join indicate an additional three, unresolved split cation positions. Inspection of the refinement output shows that As12 has one principal mean square atomic displacement about 2–3 times larger (0.1340 Å^2) than the other values for As (0.0392–0.0862 Å^2). As shown in Figure 8, the thermal ellipsoid of As12 is strongly elongated in the direction S22-As12-S27. The Pb-S bond-pairs (of Pb5a and Pb13a) show bond distances significantly longer compared to As-S but falling short of the Pb-S hyperbola in Figure 7, indicating the average nature of the sulfur ligand positions involved.

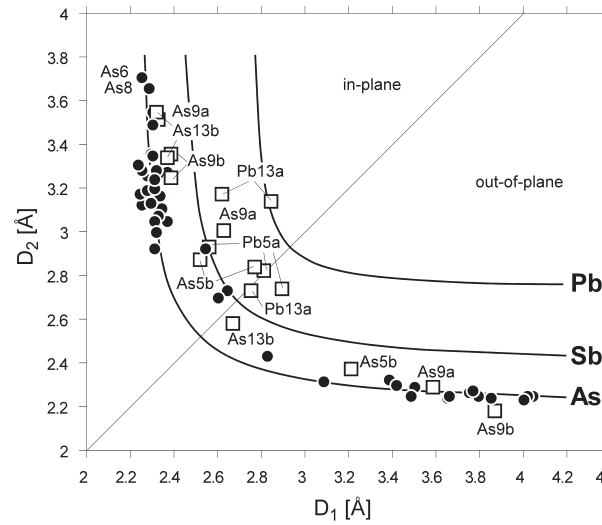

FIGURE 7. Calculated element specific bond-length hyperbolae for pairs of opposing bonds, taken from Berlepsch et al. (2001), with individual bond-length data of sartorite added. Each pair of bond-lengths consists of a short (x_n) and an opposing long (y_n) M-S bond distance (where $x_n < y_n$ and $n = 1, 2, 3$). The bond pairs (x_1y_1) and (x_2y_2) lay in the $(100)_{SnS}$ planes and the bond pair (y_3x_3) is normal to it. $D_1 = x_1, x_2, y_3$ and $D_2 = y_1, y_2, x_3$ defining the points P_1 (x_1y_1) and P_2 (x_2y_2) above and P_3 (y_3x_3) below the median line for each coordination polyhedra. Filled circles indicate As-S; empty squares indicate split positions (M5, As9, M13; see text for details).

Different hypothetical sartorite superstructures

From a topological point of view, the $(100)_{SnS}$ layers of the sartorite substructure (×9) and of the sartorite superstructure (Fig. 5) are identical in about two thirds of all polyhedra (i.e., all *Z*-type polyhedra and all polyhedra with As in the trapezoids attached "sideways"). The missing S position and the "top/bottom" attachment of S via short As-S bonds are the most prominent differences. The latter is needed for the crankshaft formation and it is interesting to see that, with the exception of As2 and As3, the positions M5, As9, As12, M13, As16, and As17 are all somehow "disturbed," i.e., they are either split and/or substituted (M5, As9, M13) or the position of the As-S bond pairs in Figure 5 suggests split but unresolved As positions (As12, As16, As17; cf. discussion above).

Although sartorite usually has an incommensurate structure and any "lock-in phase" is rather incidental, we believe that other commensurate superstructures of sartorite, differing from ninefold, can exist. The array of crankshaft chains could probably be both shortened and enlarged. In the first case a sevenfold superstructure can be imagined in which the $(100)_{SnS}$ type layer has 2 fewer PbS and 2 fewer As_2S_3 units, compared to the $(100)_{SnS}$ type layer in Figure 5 (e.g., removal of Pb8, Pb9, As15–As18, and S28–S35). Similarly, units of 2 PbS and 2 As_2S_3 could be added to the $(100)_{SnS}$ type layer and 11-fold, 13-fold etc.

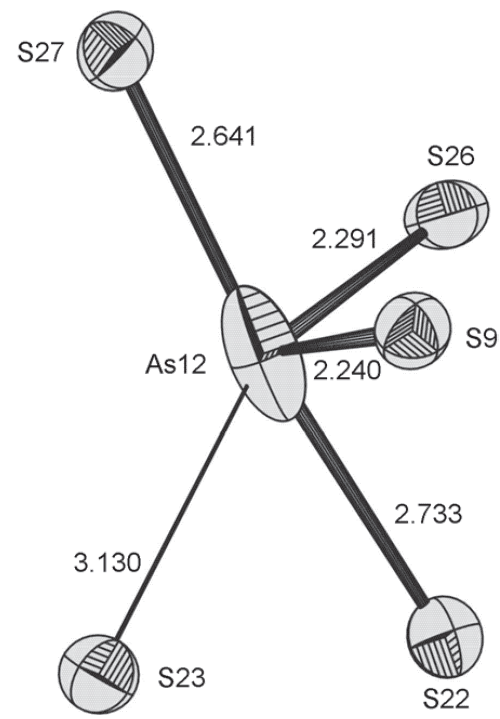

FIGURE 8. $As12S_5$ semi-polyhedron ("square" pyramid with a trapezoidal basis; cf. Fig. 5 right side). The thermal ellipsoid of As is elongated in the direction S27-As12-S22, indicating superimposed but unresolved As positions. Distances are given in angstroms. See text for details.

superstructures constructed. To which degree cation (and eventually S) substitution would have to accompany such superstructure formation remains unclear at this time.

ACKNOWLEDGMENTS

S. Graeser (Basel) kindly provided us with A. Edenharter's unpublished electron microprobe data for a "red" sartorite from the new Lengenbach quarry. We thank H. Effenberger (Vienna) and G. Ferraris (Turin) for their careful reviews and G. Giester (Vienna) for the quick handling of the manuscript.

REFERENCES CITED

Anthony, J.W., Bideaux, R.A., Bladh, K.W., and Nichols, M.C. (1990) Handbook of Mineralogy. Mineral Data Publishing, Tucson, Arizona, 1, 588 p.

Bannister, E.A., Pabst, A., and Vaux, G. (1939) The crystallography of sartorite. Mineralogical Magazine, 25, 264–270.

Baumhauer, H. (1895) Über den Skleroklas von Binn. Sitzungsberichte der Akademie der Wissenschaften, Berlin, 12, 243–252.

Berlepsch, P., Miletich, R., and Armbruster, T. (1999) The crystal structures of synthetic KSb_5S_8 and $(Tl_{0.598},K_{0.402})Sb_5S_8$ and their relation to parapierrotite ($TlSb_5S_8$). Zeitschrift für Kristallographie, 214, 57–63.

Berlepsch, P., Makovicky, E., and Balić-Žunić, T. (2001) Crystal chemistry of sartorite homologues and related sulfosalts. Neues Jahrbuch für Mineralogie, Abhandlungen, 176, 45–66.

Berlepsch, P., Armbruster, T., and Topa, D. (2002) Structural and chemical variations in rathite, $Pb_8Pb_{4-x}(Tl_2As_2)_x(Ag_2As_2)As_{16}S_{40}$: modulations of a parent structure. Zeitschrift für Kristallographie, 217, 11, 581–590.

Berry, L.G. (1943) New data on lead sulpharsenites from Binnental, Switzerland. American Mineralogist, 38, 330.

Brown, I.D. and Altermatt, D. (1985) Bond-valence parameters obtained from a systematic analysis of the inorganic crystal structure data-base. Acta Crystallographica, B41, 244–247.

Bruker AXS (1997) XPREP Ver. 5.1: A computer program for data preparation and reciprocal space exploration. Bruker Analytical X-ray systems, Madison, Wisconsin 53719–1173, U.S.A.

———(1998) SMART Ver. 5.0/NT: A software package for CCD detector systems. Bruker Analytical X-ray systems, Madison, Wisconsin 53719–1173, U.S.A.

———(1999) SAINT+ Ver. 6.01/NT: A computer program for data reduction. Bruker Analytical X-ray systems, Madison, Wisconsin 53719–1173, U.S.A.

Choi, K-S. and Kanatzidis, M.G. (2000) Sulfosalts with alkaline earth metals. Centrosymmetry *vs* acentric interplay in $Ba_3Sb_{4.66}S_{10}$ and $Ba_{2.62}Pb_{1.38}Sb_4S_{10}$ based on the Ba/Pb/Sb ratio. Phases related to arsenosulfide minerals of the rathite group and novel polysulfide $Sr_6Sb_6S_{17}$. Inorganic Chemistry, 39, 5655–5662.

Cordier, G. and Schäfer, H. (1979) Zur Darstellung und Kristallstruktur von $BaSb_2Se_4$. Zeitschrift für Naturforschung, Teil B, Anorganische Chemie, 34, 1053–1056.

Cordier, G., Schwidetzky, C. and Schäfer, H. (1984) New SbS_2 strips in the $BaSb_2S_4$ structure. Journal of Solid State Chemistry, 54, 84–88.

Hofmann, B.A. and Knill, M.D. (1996) Geochemistry and genesis of the Lengenbach Pb-Zn-As-Tl-Ba mineralization, Binn valley, Switzerland. Mineralium Deposita, 31, 319–339.

Hofmann, B.A., Graeser, S., Imhof, T., Sicher, V., and Stalder, H.A. (1993) Mineralogie der Grube Lengenbach. Jahrbuch des Naturhistorischen Museums Bern, 11, 3–90.

Hummel, W. and Armbruster, T. (1987) Tl^{1+}, Pb^{2+}, and Bi^{3+} bonding and ordering in sulfides and sulfosalts. Schweizerische Mineralogische und Petrographische Mitteilungen, 67/3, 213–218.

Iitaka, Y. and Nowacki, W. (1961) Refinement of the pseudo crystal structure of scleroclase, $PbAs_2S_4$. Acta Crystallographica, 14, 1291–1292.

Jambor, J.L. (1967) New lead sulfantimonides from Madoc, Ontario. II. Mineral descriptions. Canadian Mineralogist, 9, 191–213.

Laroussi, A., Moëlo, Y., Ohnstetter, D., and Ginderow, D. (1989) Argent et thallium dans les sulfosels de la série de la sartorite (gisement de Lengebach, Vallée de Binn, Suisse). Comptes Rendus de l'Académie des Sciences, Paris. Série II, 308, 927–933.

Le Bihan, M.-Th.(1962) Étude structurale de quelques sulfures de plomb et d'arsénic naturels du gisement de Binn. Bulletin de la Société française de minéralogie et de cristallographie, 85, 15–47.

Makovicky, E. (1967) Bemerkungen zu der Systematik und Mineralogie der Sulfosalze der Metalle der 5. Gruppe Geologická Sbornik, 15, 39–64.

———(1985) The building principles and classification of sulphosalts based on the SnS-archetype. Fortschritte der Mineralogie, 63, 45-89.

———(1997) Modular crystal chemistry of sulphosalts and other complex sulphides. In Merlino, S., Ed., Modular aspects of minerals, 1, p. 237–271. EMU Notes in Mineralogy, Eötvös University Press, Budapest.

Makovicky, E. and Balić-Žunić, T. (1998) New measure of distortion for coordination polyhedra. Acta Crystallographica, B54, 766–773.

Moëlo, Y., Makovicky, E., and Karup-Møller, S. (1984) New data on the minerals of the andorite group. Neues Jahrbuch für Mineralogie Monatshefte, 4, 175–182.

Nowacki, W. and Bahezre, C. (1963) Die Bestimmung der chemischen Zusammensetzung einiger Sulfosalze aus dem Lengenbach (Binnatal, Kt. Wallis) mit Hilfe der elektronischen Mikrosonde. Schweizerische Mineralogische und Petrographische Mitteilungen, 43, 407–411.

Nowacki, W., Iitaka, Y., and Bürki, H. (1960) Structural investigations on sulfosalts from the Lengenbach, Binn valley, Switzerland. Acta Cristallographica, 13, 1006–1007.

Nowacki, W., Iitaka, Y., Bürki, H., and Kunz., V. (1961) Structural investigations on sulfosalts from the Lengenbach, Binn valley (Ct. Wallis), Part 2. Schweizerische Mineralogische und Petrographische Mitteilungen, 41, 103–116.

Ozawa, T. (1993) Chemical compositions of some sulphosalts in the Pb-As-S system. Abstracts, Annual Meeting of the Mineralogical Society of Japan, 101.

Ozawa, T. and Takéuchi, Y. (1993) X-ray and electron diffraction study of sartorite—a periodic antiphase boundary structure and polymorphism. Mineralogical Journal, 16, 358–370.

Ozawa, T. and Tachikawa, O. (1996) A transmission electron microscope observation of 138Å period in Pb-As-S sulfosalts. Mineralogical Journal, 18, 97–101.

Palache, C., Bermann, H., and Frondel, C. (1944) Dana's system of Mineralogy, 7th edition. John Wiley and Sons, New York, 1, 478–480.

Pring, A. (2001) The crystal chemistry of the sartorite group minerals from Lengenbach, Binntal, Switzerland—a HRTEM study. Schweizerische Mineralogische und Petrographische Mitteilungen, 81, 69–87.

Pring, A. and Graeser, S. (1994) Polytypism in baumhauerite. American Mineralogist, 79, 302–307.

Pring, A., Williams, T., and Withers, R. (1993) Structural modulation in sartorite: an electron microscopy study. American Mineralogist, 78, 619–626.

Sawada, H., Kawada, I., Hellner, E., and Tokonami, M. (1987) The crystal structure of senandorite (andorite VI): lead silver antimony sulfide ($PbAgSb_3S_6$). Zeitschrift für Kristallographie, 180, 141–150.

Sheldrick, G.M. (1997a) SHELXS–97. A computer program for crystal structure determination. University of Göttingen, Germany.

———(1997b) SHELXL–97. A computer program for crystal structure refinement. University of Göttingen, Germany.

Solly, R.H. and Jackson, B.A. (1902) Sulpharsenites of lead from Binnenthal. Mineralogical Magazine, 12, 282–297.

Trechmann, C.O. (1907) Crystallography of sartorite from Binn. Mineralogical Magazine, 14, 212–229.

Trömel, M. (1981) Abstandskorrelationen bei der Tellur(IV)-Sauerstoff- und Antimon(III)-Sauerstoff-Koordination. Zeitschrift für Kristallographie, 154, 338–339.

vom Rath, G. (1864) Mineralogische Mitteilungen. Annalen der Physik und Chemie, 122, 371–399.

MANUSCRIPT RECEIVED MAY 22, 2002
MANUSCRIPT ACCEPTED JULY 25, 2002
MANUSCRIPT HANDLED BY GERALD GIESTER